Asymmetric beams and CMB statistical anisotropy

PHYSICAL REVIEW D **81,** 103003 (2010)

Asymmetric beams and CMB statistical anisotropy

Duncan Hanson,[1] Antony Lewis,[1,2] and Anthony Challinor[1,3]

[1]*Institute of Astronomy and Kavli Institute for Cosmology Cambridge, University of Cambridge, Madingley Road, Cambridge CB3 OHA, United Kingdom*

[2]*Department of Physics & Astronomy, Pevensey II Building, University of Sussex, Falmer, Brighton BN1 9QH, United Kingdom*

[3]*DAMTP, Centre for Mathematical Sciences, University of Cambridge, Wilberforce Road, Cambridge CB3 OWA, United Kingdom*

(Received 3 March 2010; published 12 May 2010)

Beam asymmetries result in statistically anisotropic cosmic microwave background (CMB) maps. Typically, they are studied for their effects on the CMB power spectrum, however they more closely mimic anisotropic effects such as gravitational lensing and primordial power asymmetry. We discuss tools for studying the effects of beam asymmetry on general quadratic estimators of anisotropy, analytically for full-sky observations as well as in the analysis of realistic data. We demonstrate this methodology in application to a recently detected 9σ quadrupolar modulation effect in the WMAP data, showing that beams provide a complete and sufficient explanation for the anomaly.

DOI: 10.1103/PhysRevD.81.103003 PACS numbers: 98.70.Vc, 98.80.Es

The cosmic microwave background (CMB) is a powerful probe for both modern and future cosmology: its rotationally invariant power spectra have been instrumental in hammering out the details of the current concordance model, its non-Gaussianities have the potential to discriminate between various early-universe models, and its statistical anisotropies can be used to probe astrophysically interesting secondary effects such as gravitational lensing.

We observe the CMB through the convolution of an instrumental beam, an effect which must be carefully treated in analysis. Qualitatively, the effects of beams are twofold: (i) they suppress structures on scales smaller than the beam size; and (ii) if the beams are asymmetric, they can introduce statistical anisotropies into the observed CMB which can bias estimators for other anisotropic signals. The purpose of this paper is to collect results on the simulation of beam effects, and to present fast, accurate techniques for forecasting and correcting the effects of beams on estimators of statistical anisotropy. In Sec. I we present a model of beam asymmetries and we discuss the covariance which beams produce in the observed CMB in Sec. II. In Sec. III we derive the effects of the anisotropic covariance on anisotropy estimators, and in Sec. IV we illustrate this discussion by applying these techniques to study the effects of beams on the highly significant quadrupolar modulation effect in the WMAP data. Our conclusions are collected in Sec. V. The effect of beam asymmetries on the estimated power spectrum of the CMB for general survey geometries is discussed in Appendix B.

I. MODEL

In a realistic CMB observation, the effective sky signal at each point in the time-ordered data (TOD) is a convolution of the true sky signal with the experimental beam, oriented according to the scan strategy. Schematically, we have

$$T_i = \int_{S^2} d\Omega r_i(\Omega)\Theta(\Omega) + n_i, \tag{1}$$

where T_i is the temperature for time-step i in the TOD, $\Theta(\Omega)$ is the underlying CMB signal, $r_i(\Omega)$ is the beam response, and n_i is the instrumental noise. For the purposes of compact notation we will abbreviate $\int_{S^2} d\Omega$ as $\int$ for the remainder of this paper. The integral in Eq. (1) can be performed by brute force in real space using interpolation on pixelized maps of the beam and sky [1]. For this approach to be computationally feasible, the beam must be assumed zero outside some small patch where its response is peaked, and so it is difficult to study sidelobe effects with this approach, although it can be quite fast.

In this work, we will find it more useful to work in harmonic space, where the effects of beams are easier to study analytically. We begin by writing the beam response as a harmonic sum. If we center the beam at the north pole, with some fiducial beam axis aligned along the $+x$ axis (the $\phi = 0$ meridian), and expand it in spherical harmonics b_{lm}, then the beam at location Ω for the ith TOD observation is given by (e.g. [2])

$$r_i(\Omega) = \sum_{s=-s_{\max}}^{s_{\max}} \sum_{l=|s|}^{l_{\max}} \sum_{m=-l}^{l} D^l_{ms}(\phi_i, \theta_i, \alpha_i) b_{ls0} Y_{lm}(\Omega). \tag{2}$$

For the purposes of compact notation we will drop the summation limits in what follows. The limits themselves will be discussed later. The action of the Wigner-D matrix can be visualized as follows: imagine fixing the coordinate system in space and performing right-handed rotations of the beam image about the z axis by an angle α_i, then about the y axis by an angle θ_i, and finally about the z axis by an angle ϕ_i. The first rotation gives the beam its orientation: α_i is the angle of the fiducial beam axis, measured from the southern side of the meridian which passes through the pixel location (θ_i, ϕ_i) assigned to the observation. We use ${}_sY_{lm}$ to denote a spin-weighted spherical harmonic, of

which the standard spherical harmonics are a special case with $s = 0$. Unless otherwise noted, the harmonics should be taken as functions of Ω. We can then rewrite Eq. (1) as

$$T_i = \sum_{lms} D^l_{-ms}(\phi_i, \theta_i, \alpha_i) b_{ls} (-1)^m \Theta_{lm} + n_i$$
$$= \sum_{lms} e^{-is\alpha_i} B_{ls} \Theta_{lms} Y_{lm}(\theta_i, \phi_i) + n_i. \quad (3)$$

In the second step we have used the close relationship between Wigner-D functions and the spin-weighted spherical harmonics [3], and introduced the beam transfer function B_{ls} given by

$$B_{ls} = \sqrt{\frac{4\pi}{2l+1}} b_{ls}. \quad (4)$$

For a beam which is normalized to have unit response to a monopole, $B_{00} = 1$. We shall refer to the $s = 0$ coefficients of the beam as the symmetric part, as they represent the component of the beam which depends only on the radial distance from its center. The $s \neq 0$ coefficients encapsulate beam asymmetry. On scales much smaller than the beam size, B_{ls} becomes very small, which effectively band limits $B_{ls}\Theta_{lm}$. This scale determines $l_{\max}$. The evaluation of Eq. (3) may then be performed in $\mathcal{O}(s_{\max} l^2_{\max})$. To perform this convolution for each time step in the TOD is in general prohibitively expensive, and some approximations must be made. There are several possible approaches:

(1) The convolution can be computed over a grid covering the full rotation group with fast-Fourier-transforms for the Euler angles ϕ and α and, optionally, for θ [4]. The TOD can be obtained by interpolation off this grid.

(2) If the beam may be represented using a small number of symmetric basis functions, each of these may be rapidly convolved in harmonic space and then sampled based on the location and orientation of these basis functions for each sample in the TOD [5]. The difficulty here is the ability to represent the beam as a sum of symmetric functions. Note that in the limit that the beam is represented as a sum of delta functions, this approach is conceptually the same as real-space integration.

We note the above approaches for completeness. In this work, we will use a popular [6–9] map-based approach based on the assumption that the TOD noise is uncorrelated on the time scales which separate pixel visits. In this case, it is a good approximation to the mapmaking process (in the absence of beam deconvolution [10]) to take

$$\tilde{\Theta}(\Omega_p) + n(\Omega_p) = \sum_{i \in p} T_i / H_p, \quad (5)$$

where $\tilde{\Theta}$ is an effectively observed sky, $n(\Omega_p)$ is a noise map, and H_p is the number of elements in the sum, which is taken over all hits assigned to pixel p, with center at Ω_p. This approach can also be used for differencing experiments, which suppress correlations between TOD samples by mapmaking from the difference between two nearly identical detectors, to remove common mode fluctuations. In this case, one can use an effective beam which is a hit-weighted sum of the two beams which are differenced [11].

In conjunction with Eq. (3), the sum of Eq. (5) can be seen to effect a Fourier transform of the distribution of orientation angles, with an effective observed sky given by [6]

$$\tilde{\Theta}(\Omega_p) = \sum_s w(\Omega_p, -s) \Big[\sum_{lm} B_{ls} \Theta_{lms} Y_{lm}(\Omega_p) \Big], \quad (6)$$

where the details of the scan strategy are contained in the spin $-s$ field,

$$w(\Omega_p, -s) = \sum_{i \in p} e^{-is\alpha_i} / H_p. \quad (7)$$

Since ${}_sY_{lm}$ involves s (spin-weighted) derivatives of the Y_{lm}, each term in the s sum is the real-space product of the scan strategy and beam-filtered derivatives of the CMB. For a beam which is approximately azimuthally symmetric, or a scan strategy which broadly distributes the orientation angles, $w(\Omega_p, -s) B_{ls}$ falls off sharply with s, and it follows that calculation of only the lowest s terms suffice to give a good approximation to the beam-convolved map. This determines an effective $s_{\max}$ which can be much less than that naively required to describe accurately the beam in Eq. (2).

Given a scan strategy, Eq. (6) provides an $\mathcal{O}(s_{\max} l^3_{\max})$ method to compute effectively the sky observed by an experiment with an asymmetric beam B_{ls} and given scan strategy $w(\Omega_p, s)$. This approximation is useful not only for its speed, but also to gain an intuitive analytical understanding of beam effects, which we proceed to discuss in the following sections.

II. COVARIANCE

Beam effects are linear in the underlying CMB, and so do not affect its (assumed) Gaussianity. For Gaussian models, the statistics of the observed CMB remain completely characterized by its covariance. The effect of beams is simply to introduce statistical anisotropies which give off-diagonal and m-dependent contributions to the covariance.

In harmonic space the beam-convolved sky is given by

$$\tilde{\Theta}_{l'm'} = \sum_{LMS} \sum_{lm} B_{lS} \Theta_{lm-S} {}_Sw_{LM} \int {}_{-S}Y_{LM0} Y^*_{l'm'S} Y_{lm}, \quad (8)$$

where

$${}_Sw_{LM} = \int w(\Omega, S)\, {}_SY^*_{LM} \quad (9)$$

are the spin-S multipoles of $w(\Omega, S)$.

The covariance of the beam-convolved CMB may then be written as

$$\tilde{C}_{l_1m_1l_2m_2} = \langle \tilde{\Theta}_{l_1m_1} \tilde{\Theta}^*_{l_2m_2} \rangle = \delta_{l_1l_2}\delta_{m_1m_2} B^2_{l_10} C^{\Theta\Theta}_{l_1} + (-1)^{m_2} \Delta_{l_1m_1l_2-m_2}. \quad (10)$$

The $\Delta_{l_1m_1l_2m_2}$ term contains the part of the covariance which is due to beam asymmetries. We further split it into two terms, such that $\Delta = \Delta^{(1)} + \Delta^{(2)}$. The $\Delta^{(1)}$ terms are those which couple an $s = 0$ mode of the convolution with an $s \neq 0$ mode. The notation arises because we think of them being first order in any beam asymmetry:

$$\Delta^{(1)}_{l_1m_1l_2m_2} = \sum_{S\neq 0}\sum_{LM} {}_Sw_{LM} \int {}_SY^*_{LM} [{}_0Y_{l_1m_1S} Y_{l_2m_2} B^*_{l_2S} B_{l_20} C^{\Theta\Theta}_{l_2} + (1 \leftrightarrow 2)]. \quad (11)$$

The $(1 \leftrightarrow 2)$ represents the interchange of l_1, l_2 and m_1, m_2 in the preceding expression. The $\Delta^{(2)}$ terms couple two $s \neq 0$ modes:

$$\Delta^{(2)}_{l_1m_1l_2m_2} = \sum_{\substack{S_1\neq 0\\ S_2\neq 0}}\sum_{lm} (-1)^m B_{lS_1} B_{lS_2} C^{\Theta\Theta}_l \times \sum_{L_1M_1} {}_{-S_1}w_{L_1M_1} \left(\int {}_{-S_1}Y_{L_1M_1} ({}_0Y^*_{l_1m_1})_{S_1} Y_{l-m} \right) \times \sum_{L_2M_2} {}_{-S_2}w_{L_2M_2} \left(\int {}_{-S_2}Y_{L_2M_2} ({}_0Y^*_{l_2m_2})_{S_2} Y_{lm} \right). \quad (12)$$

Traditionally, CMB analyses have focused on the power spectrum, or average diagonal elements of the covariance matrix for each l. The $\Delta^{(1)}$ term evaluates to zero for these elements, however, and so the effects of beam asymmetries on the power spectrum are due solely to the $\Delta^{(2)}$ terms. For estimators of statistical anisotropy, however, the dominant contributions to Δ are expected to be the $\Delta^{(1)}$ terms, which involve only one power of $B_{l(s\neq 0)}$. Beam asymmetries therefore have quantitatively different effects on the power spectrum and on anisotropy estimators. A further important difference is that beam asymmetries are only an issue for the power spectrum on small scales, but, due to mode coupling, they can still be important when reconstructing large-scale modes of any statistical anisotropy. Note that the above arguments only apply exactly on the full-sky with uniform pixel weighting. For pseudo-C_l power spectra on a cut sky or with anisotropic weighting (for example, to mitigate inhomogeneous pixel noise), the beam anisotropies can couple with the asymmetry introduced by the weights, which gives $\Delta^{(1)}$ a contribution to the power spectrum. However, this is only significant near strong inhomogeneities in the pixel weights, and is therefore generally suppressed. For the remainder of this paper, we will focus on the effects of beams on anisotropy estimators. The effects on the power spectrum are discussed in Appendix B; see also [11].

III. ANISOTROPY ESTIMATORS

The CMB is assumed to be statistically isotropic to a good approximation, but there may be small contributions to the covariance from a variety of effects, such as gravitational lensing (if the lensing potential is considered as fixed, see e.g. [12] for a review), inhomogeneous reionization (if the reionization history is fixed, see e.g. [13]), Doppler modulation [14], or more exotic statistical anisotropy (e.g. [15] and references therein). Following the notation introduced in the previous section, we will write the CMB covariance as

$$\langle \Theta_{l_1m_1} \Theta^*_{l_2m_2} \rangle = \delta_{l_1l_2}\delta_{m_1m_2} C^{\Theta\Theta}_{l_1} + \sum_i (-1)^{m_2} \Delta^{(i)}_{l_1m_1l_2-m_2}, \quad (13)$$

where i labels the various physical effects that contribute to the anisotropy.

If we assume that the anisotropy from each effect i is sourced linearly by multipoles ${}_{S^i}f^{(i)}_{LM}$ with spin weights $\{S^i\}$ that satisfy $[{}_{S^i}f^{(i)}_{LM}]^* = (-1)^{S^i+M}\,{}_{-S^i}f^{(i)}_{L-M}$, then covariance under rotations (i.e. the requirement that if Θ is rotated, f_{LM} must rotate in tandem) and parity $[{}_{S^i}f^{(i)}_{LM} \rightarrow (-1)^{S^i+L}\,{}_{-S^i}f^{(i)}_{LM}]$ generally requires that each term in Eq. (13) has the form

$$\Delta^{(i)}_{l_1m_1l_2m_2} = \sum_{S^iLM} {}_{S^i}f^{(i)}_{LM} \sum_{s_1} \left(\int {}_{S^i}Y^*_{LMs_1} Y_{l_1m_1s_2} Y_{l_2m_2} \right) \times W^{(i)}_{S^i,s_1}(l_1, l_2, L), \quad (14)$$

where $W^{(i)}_{S^i,s_1}(l_1, l_2, L) = (-1)^{S^i} W^{(i)}_{-S^i,-s_1}(l_1, l_2, L)$ is a weight function which describes the way in which the anisotropy field couples the Θ multipoles, while s_1 and $s_2 \equiv S^i - s_1$ label different partitions of the spin S^i between two spin-weighted harmonics.[1] Typically, one of s_1 or s_2 is zero since we are dealing here with the spin-0

[1] Two examples may help to solidify the notation. For lensing, $\Theta \rightarrow \Theta + d^a\nabla_a\Theta$ to first order in the lensing deflection d^a. This gives a covariance with nonzero weights

$$W^{(\mathrm{lens})}_{\pm1,\pm1}(l_1, l_2, L) = \mp \frac{C^{\Theta\Theta}_{l_1}}{2\sqrt{l_1(l_1+1)}}$$

$$W^{(\mathrm{lens})}_{\pm1,0}(l_1, l_2, L) = \mp \frac{C^{\Theta\Theta}_{l_2}}{2\sqrt{l_2(l_2+1)}},$$

and $\{{}_Sf^{(\mathrm{lens})}_{LM}\} = \{{}_{\pm1}d_{LM}\}$ are the spin-weight multipoles of the deflection field. Note that we have not assumed that d^a is a gradient here. For beam asymmetries with ${}_Sf^{(\mathrm{beams})}_{LM} = {}_Sw_{LM}$, the nonzero weights are $W^{(\mathrm{beams})}_{S,0}(l_1, l_2, L) = B^*_{l_2S} B_{l_20} C^{\Theta\Theta}_{l_2}$ and $W^{(\mathrm{beams})}_{S,S}(l_1, l_2, L) = B^*_{l_1S} B_{l_10} C^{\Theta\Theta}_{l_1}$.

temperature. It can be seen that the $\Delta^{(1)}$ term of the beam covariance in the previous section is of this form (although the smaller $\Delta^{(2)}$ term is not). The $\Delta^{(i)}_{l_1m_1l_2m_2}$ are symmetric under $(1 \leftrightarrow 2)$ so we may take $W^{(i)}_{S^i,s_1}(l_1, l_2, L) = W^{(i)}_{S^i,s_2}(l_2, l_1, L)$. Moreover, $(-1)^{m_2}\Delta^{(i)}_{l_1m_1l_2-m_2}$ is Hermitian under $(1 \leftrightarrow 2)$ which gives rise to the spin-flip symmetry

$$W^{(i)}_{S^i,s_1}(l_1, l_2, L) = (-1)^{S^i} W^{(i)*}_{-S^i,-s_2}(l_2, l_1, L). \tag{15}$$

Note that the quantity $W(l_1, l_2, L)_S f_{LM}$ is essentially equivalent to the bipolar spherical harmonic coefficients, $A^{LM}_{l_1l_2}$, of Hajian and Souradeep [16]. The formalism which we will use here and the bipolar spherical harmonic formalism can be thought of as two different representations of the same symmetry relations, analogous to e.g. Clebsch-Gordan coefficients and Wigner $3j$ symbols. Similarly, their relative benefits depend on the use. For calculations, the quadratic estimator approach often results in simpler expressions, but the $A^{LM}_{l_1l_2}$ can prove more useful for blind searches, or for gaining insight into the physical interpretation of the anisotropies and the relationships between different models [17].

As discussed in [15], optimal quadratic maximum-likelihood estimators can be constructed for ${}_S f_{LM}$, under the assumption that their effects are perturbative. The estimators approximately maximize the Gaussian log-likelihood $\mathcal{L}$ with respect to the ${}_S f_{LM}$, so that they solve $\partial\mathcal{L}/\partial_S f_{LM} = 0$. The solution is constructed from a set of quadratic building blocks ${}_{S^i}h^{(i)}_{LM}$, each of the form

$$\begin{aligned} {}_{S^i}h^{(i)}_{LM} &= \frac{1}{2}\sum_{l_1m_1,l_2m_2} \bar{\Theta}_{l_1m_1}\left(\frac{\partial\Delta^{(i)}_{l_1m_1l_2m_2}}{\partial_{S^i} f^{(i)}_{LM}}\right)^* \bar{\Theta}_{l_2m_2} \\ &= \frac{1}{2}\sum_{l_1m_1,l_2m_2,s_1}\left[\int {}_{S^i}Y^*_{LMs_1} Y_{l_1m_1s_2} Y_{l_2m_2}\right] \\ &\quad \times W^{(i)*}_{S^i,s_1}(l_1, l_2, L)\bar{\Theta}_{l_1m_1}\bar{\Theta}_{l_2m_2}, \end{aligned} \tag{16}$$

where $\bar{\Theta}_{lm}$ is the inverse-variance filtered observed sky (in general the observed sky premultiplied by the signal-plus-noise inverse covariance including all anisotropic contributions to the covariance that do not depend on the set of parameters that are being estimated). The inverse-variance filtering can be performed quickly using conjugate descent with a good preconditioner, the best to date being that of [6]. The estimator for ${}_{S^i}f^{(i)}_{LM}$ is then given by

$${}_{S^i}\hat{f}^{(i)}_{LM} = \sum_{L'M'jS^j} \mathcal{F}^{-1}_{iS^iLM,jS^jL'M'}\left[{}_{S^j}h^{(j)}_{L'M'} - \langle {}_{S^j}h^{(j)}_{L'M'}\rangle\right], \tag{17}$$

where the ensemble average is taken over realizations of the CMB and noise. The "mean-field" term $\langle {}_{S^i}h^{(i)}_{LM}\rangle$ subtracts off anisotropy due to anisotropic noise, sky cuts, and known anisotropic components of the covariance (e.g. beam asymmetries). The matrix $\mathcal{F}^{-1}$ is the inverse of the Fisher matrix, which is calculated as

$$\begin{aligned} \mathcal{F}_{iS^iLM,jS^jL'M'} &= \frac{1}{2}\sum_{l_1m_1,\ldots,l_4m_4} (-1)^{m_1+m_2} C^{-1}_{l_1m_1l_2m_2} \\ &\quad \times \left(\frac{\partial\Delta^{(i)}_{l_3m_3l_2-m_2}}{\partial_{S^i} f^{(i)}_{LM}}\right)^* C^{-1}_{l_3m_3l_4m_4} \frac{\partial\Delta^{(j)}_{l_4m_4l_1-m_1}}{\partial_{S^j} f^{(j)}_{L'M'}}, \end{aligned} \tag{18}$$

where C^{-1} is the inverse covariance matrix used to construct $\bar{\Theta}_{lm}$. The Fisher matrix can be shown to equal the covariance of the ${}_{S^i}h^{(i)}_{LM}$:

$$\mathcal{F}_{iS^iLM,jS^jL'M'} = \langle {}_{S^i}h^{(i)}_{LM\,S^j}h^{(j)*}_{L'M'}\rangle - \langle {}_{S^i}h^{(i)}_{LM}\rangle\langle {}_{S^j}h^{(j)*}_{L'M'}\rangle. \tag{19}$$

For an observation and underlying CMB that are statistically isotropic (e.g. full-sky coverage with homogeneous noise levels and symmetric beams), rotational symmetry requires that the inverse-variance filtered CMB has a diagonal covariance

$$\langle \bar{\Theta}_{l_1m_1}\bar{\Theta}^*_{l_2m_2}\rangle = \frac{\delta_{l_1l_2}\delta_{m_1m_2}}{C^{\rm tot}_{l_1}}\ \text{(iso)}, \tag{20}$$

where $1/C^{\rm tot}_l$ is the inverse-variance filter. This propagates to the Fisher matrix $\mathcal{F}$, which is then also diagonal in L, and independent of M:

$$\begin{aligned} \mathcal{F}^{\rm iso}_{iS^iLM,jS^jL'M'} &= \delta_{LL'}\delta_{MM'}\sum_{l_1l_2s_1s'_1} (-1)^{S^i+S^j} \\ &\quad \times \frac{(2l_1+1)(2l_2+1)}{8\pi C^{\rm tot}_{l_1}C^{\rm tot}_{l_2}} W^{(i)*}_{S^i,s_1}(l_1, l_2, L) \\ &\quad \times W^{(j)}_{S^j,s'_1}(l_1, l_2, L)\begin{pmatrix} l_1 & l_2 & L \\ -s_1 & -s_2 & S^i \end{pmatrix} \\ &\quad \times \begin{pmatrix} l_1 & l_2 & L \\ -s'_1 & -s'_2 & S^j \end{pmatrix}. \end{aligned} \tag{21}$$

The isotropic Fisher matrix is chiefly useful for forecasting purposes. In practice, inhomogeneous sky coverage and foreground cuts mean that it should be estimated from simulations.

If the weights are separable, such that $W(l_1, l_2, L) = W_1(l_1)W_2(l_2)W_L(L)$, or can be decomposed as a sum of separable terms, then these estimators have fast position-space forms with computational cost $\mathcal{O}(l^3_{\rm max})$, and the isotropic Fisher matrix can be evaluated in $\mathcal{O}(l^2_{\rm max})$ [13].

It can be seen clearly from Eq. (11) that these tools apply to the covariance produced by beam asymmetries. Optimal estimators could, for example, be formed to reconstruct the components of ${}_S w_{LM}$ for each S. In practice, the instrumental scan strategy is fixed and asymmetric beams act as a source of bias for other anisotropy estimators, which have the form of Eq. (16). In this view, beams simply make a contribution to the covariance of the observed sky. They

should be incorporated into the inverse-variance filtering operation and the mean-field subtraction. For realistic observations, this can be done easily as the inverse-variance filtering step is done using conjugate descent, and requires only a fast method to apply the beam effects, such as that provided by Eq. (8). This is demonstrated at the TOD level in [10], for example. The mean-field can be determined straightforwardly from simulations. Analytic calculations are also feasible if the inverse-variance filter is isotropic, and can be useful for forecasting purposes. Neglecting a known source of anisotropy in the data during mean-field subtraction will generally bias anisotropy estimators for other effects. Explicitly, the mean-field bias on an estimator ${}_{S^j}\hat{f}^{(j)}_{LM}$ with weight function $W^{(j)}_{S^j,s_1}(l_1, l_2, L)$ by a contaminant i with covariance as in Eq. (14) is

$$\langle {}_{S^j}h^{(j)}_{LM}\rangle = {}_{S^i}f^{(i)}_{LM}\sum_{l_1 l_2 S^i s_1 s_1'}(-1)^{S^i+S^j}\frac{(2l_1+1)(2l_2+1)}{8\pi C^{\rm tot}_{l_1}C^{\rm tot}_{l_2}} \times W^{(i)}_{S^i,s_1}(l_1,l_2,L)\begin{pmatrix} l_1 & l_2 & L \\ -s_1 & -s_2 & S^i\end{pmatrix} \times W^{(j)*}_{S^j,s_1'}(l_1,l_2,L)\begin{pmatrix} l_1 & l_2 & L \\ -s_1' & -s_2' & S^j\end{pmatrix}. \quad (22)$$

A nice feature of this result is that the bias rather directly traces the spatial distribution of the contaminant: the bias is an isotropically filtered version of the contaminant. In the case of pixel-uncorrelated anisotropic instrumental noise, for example, the mean-field simply traces the anisotropic part of the noise variance map [18]. In the case of beams, on the other hand, the mean-field traces the components of the scan strategy ${}_{S}w_{LM}$.

IV. CASE STUDY: PRIMORDIAL POWER ASYMMETRY

As an example of this machinery in action, we study a high-significance anomaly in the WMAP data, which resembles the effects of a modulation of the primordial power spectrum. Explicitly, one can construct estimators based on the covariance for a k-space modulation of the primordial power spectrum $\mathcal{P}_\chi(\mathbf{k})$ with the form

$$\mathcal{P}_\chi(\mathbf{k}) = \mathcal{P}_\chi(k)[1 + g(\hat{\mathbf{k}})]. \quad (23)$$

If we take the bi-Copernican hypothesis that the universe has no preferred orientation then the expectation is that $g(\hat{\mathbf{k}}) = 0$. However, current analyses of the WMAP maps strongly favor a model in which $g(\hat{\mathbf{k}})$ has quadrupolar components

$$g(\hat{\mathbf{k}}) = \sum_{|M|\le 2} g_{2M0}Y_{2M}(\hat{\mathbf{k}}). \quad (24)$$

Furthermore, the preferred g_{2M} are planar, with $g_{2M} \propto \delta_{M0}$ in ecliptic coordinates [15,17,19]:

$$g(\hat{\mathbf{k}}) = g_{20}\frac{1}{2}\sqrt{\frac{5}{4\pi}}(3\cos^2\theta_{\hat{\mathbf{k}}} - 1), \quad (25)$$

where $\theta_{\hat{\mathbf{k}}}$ is the angle from the ecliptic pole. This form resembles the model proposed by [20] (and other authors, e.g. [21]) which was the motivation for original detection made in [22]. A missing factor in the original version of [20] resulted in the ecliptic orientation being obscured; however, this was corrected by [15]. The ecliptic alignment of the detected effect strongly suggests an instrumental systematic or solar-system origin. The signal is present at 9σ in the W band [19], but varies strongly between detectors at the same frequency [15,17], which singles out an instrumental explanation, although [19] have also checked the contribution of zodiacal light and found a negligible effect.

Here we will continue the work of [15], using optimal quadratic maximum-likelihood estimators to study the primordial modulation effect. These estimators are often favorable to the Gibbs-sampling approach of [19,22] for their speed, and the ease with which they can be modified to test various systematic effects [15,17]. In the current application, the quadratic estimator compresses millions of correlations between thousands of observed modes to a small handful of parameters, and should be effectively indistinguishable from an exact likelihood analysis [17]. In the formalism of the previous section, the quadratic estimator for g_{2M} has $S = s_1 = 0$, and the weight function can be written as [15,23]

$$W(l_1, l_2, 2) = \frac{i^{l_1-l_2} + i^{l_2-l_1}}{2}C_{l_1 l_2}, \quad (26)$$

where the $C_{l_1 l_2}$ matrix is given by

$$C_{l_1 l_2} = 4\pi\int d\ln k\,\mathcal{P}_\chi(k)\Delta_{l_1}(k)\Delta_{l_2}(k). \quad (27)$$

The $\Delta_l(k)$ used here are the angular CMB transfer functions.

The largest expected instrumental effects which can produce ecliptic-aligned anomalies are inhomogeneous pixel noise levels and beam asymmetries. The pixel-uncorrelated component of the instrumental noise is already accounted for in current analyses, and it has been argued that these estimators are insensitive to percent-level changes in the noise amplitude [19]. We agree with this result: the mean-field for the quadratic estimator of primordial power modulation due to WMAP noise inhomogeneities is less than 1σ for all V- and W-band differencing assemblies (DAs), and so percent-level changes in the noise level do not have appreciable effects. In the bipolar power spectrum formalism, this is because inhomogeneous instrumental noise produces coefficients of the form $A^{LM}_{l_1 l_2} \propto$ const (in the notation of [17]), which more closely resembles a modulation of the *observed* power spectrum in real space than a modulation of the primordial power

spectrum in k space [17]. Anomalies are also seen in estimates of g_{2M} formed from cross correlations between maps with different noise realizations, which suggests that noise cannot be the dominant effect [15,17].

It has been argued that beams must provide at least a significant source of bias for estimates of $g(\hat{\mathbf{k}})$ [15], if not a complete explanation [17], although [19] have also studied the effects of beams and concluded that they are unimportant. Here we will address this issue using the new tools of the previous section. We obtain the coefficients of the instrumental beam directly from the WMAP five-year published beam maps [24] by a brute-force discrete harmonic transform, with beam center determined simply from the maximum pixel. For each beam map, we then scale the resulting B_{lm} such that $B_{00} = 1$, and average the A- and B-side beams together, as appropriate for simulating the effect of differencing on the final map [11]. Finally, we scale these averaged beam transfer functions at each l so that the B_{l0} components agree with the published WMAP transfer functions. These are derived from the same TOD observations of Jupiter which are used to create the beam maps, but do not suffer from pixelization effects. Without this scaling, our B_{l0} would still agree with the published values at a level of better than 1% for $l < 600$.

To get a feeling for the expected effects we begin by evaluating Eq. (22). We only calculate the bias due to the $\Delta^{(1)}$ terms of the beam covariance, however we will later verify numerically that the $\Delta^{(2)}$ terms are not significant for this application, as expected. As we are ultimately only interested in the low-l multipoles of the beam mean-field it is sufficient to have a model for the scan strategy ${}_S w_{LM}$ at low-l, and for correspondingly small S. We will initially use $s_{\max} = 6$. To calculate the ${}_S w_{LM}$ we use the analytical method of [7], outlined in Appendix A, which provides an excellent approximation to the true scan strategy on such large scales. Following the notation there, we use a toy model for WMAP, with a spin period of two minutes, a precession period of one hour, and scan angles of $\theta_b = 70°$, $\theta_p = 22.5°$. These are design values for the fiducial center of the WMAP focal plane, and were achieved with good accuracy in flight [25]. The position of the individual detectors within the focal plane does effectively vary θ_b. We have not corrected for this; however, as we will discuss, this does not significantly affect our results. The expected mean-field biases are presented in Table I, for the V- and W-band DAs. We initially limit our analysis to $l_{\max} = 400$ for comparison with earlier results. The inverse-variance filters use isotropic noise with the appropriate power spectrum. This evaluation takes only a few seconds for such low $s_{\max}$. The fast precession of the WMAP spin axis gives the scan-strategy azimuthal symmetry in ecliptic coordinates, which makes ${}_S w_{LM} \propto \delta_{M0}$. Because the bias is proportional to this quantity, it also has this azimuthal symmetry, which would explain the planar structure of the detected modulation, and the alignment of the detected effects with the ecliptic poles. The north-south symmetry of the scan strategy also restricts ${}_S w_{LM}$ to even-L. The mean-fields for $l = 2$ are predicted to be large, and detectable at many sigma. Higher multipoles ($l = 4, 6$) receive much less significant contributions from beams, and are also not observed to be anomalous in the data [15]. Thus, beams seem to be a likely explanation for the detected anomaly.

TABLE I. Analytic predictions for the beam mean-field bias to the primordial power asymmetry estimator, with $l_{\max} = 400$. The significance (σ) is given by the mean-field divided by the estimator noise.

DA	$\langle g_{20} \rangle$	(σ)	$\langle g_{40} \rangle$	(σ)	$\langle g_{60} \rangle$	(σ)
$Q1$	−0.33	(12.1)	0.030	(0.83)	−0.003	(0.07)
$Q2$	−0.33	(12.3)	0.029	(0.81)	−0.003	(0.08)
$V1$	0.17	(6.51)	0.031	(0.86)	−0.003	(0.07)
$V2$	0.17	(6.74)	0.032	(0.92)	−0.002	(0.06)
$W1$	0.27	(9.10)	0.043	(1.07)	−0.002	(0.05)
$W2$	0.31	(9.79)	0.042	(0.97)	−0.003	(0.06)
$W3$	0.33	(9.99)	0.037	(0.85)	−0.002	(0.05)
$W4$	0.27	(8.63)	0.045	(0.95)	−0.003	(0.05)

Before we move on to the analysis of the WMAP data itself, we consider some of the insights which the analytic approach makes possible. Because the detected anomaly is quadrupolar, it depends on the scan strategy only up to $S = 2$ (as there are no $L = 2$ modes for larger S). This means that if beams are the explanation they can only be sourced by the beam's dipole and ellipticity components. These modes are well constrained by the beam maps, so we expect our calculations to be quite accurate. As already mentioned, the effective θ_b which we use for our scan-strategy calculation differs for some detectors due to their position in the focal plane. We find that $\partial({}_2 w_{20})/\partial\theta_b = 2\%/\,\text{deg}$ about the fiducial value. As all of the V- and W-band detectors are clustered within 1° in azimuth of the center of the focal plane, we expect at most 2% errors in the scan-strategy coefficients. This corresponds to $<0.2\sigma$ effects for the biases which we have derived. The analytical calculations also reveal that the dominant contribution to the quadrupolar bias is given by the $S = 2$ modes, rather than $S = 1$. For our purposes, this is quite fortuitous—there are a number of opportunities in this calculation for 180° errors in the beam orientation angle, however any such errors will not significantly affect our results.

Another question which can be asked is whether it might be possible to verify the effects of beams with an estimator more optimally designed to detect them. A Fisher-matrix calculation shows that the g_{2M} estimator has a typical correlation coefficient of 0.9 with the optimal quadrupole "scan-strategy" estimator with the known WMAP beams, and so the g_{2M} estimator is effectively optimized to detect beam effects.

Finally, it is interesting to note that the bias for the Q-band data has the opposite sign of that for the V and

W bands. This effect has already been observed in the data by [19], although without explanation. It is due to the fact that the semimajor axis of the beam ellipticity for the Q band is oriented parallel to the scan direction, while the V/W axes are perpendicular [26]. A 90° rotation corresponds to a sign flip for the $S = 2$ modes of the beam which dominate the bias. This feature provides strong evidence that the dominant effect which sources the quadrupolar effect is beam asymmetries.

We now turn to the question of whether beam effects are sufficient to explain completely the quadrupole anomaly, as seems likely from the significance levels in Table I. It is straightforward to fold asymmetric beam effects directly into our analysis [15] of the WMAP five-year data [24]; we have not yet upgraded to the seven-year data, which are very consistent [17]. In the quadratic estimator formalism which we use here, the estimator mean-field and Fisher matrix are determined on the cut sky by Monte Carlo. By incorporating beam effects into the CMB simulations using Eq. (8), the Monte-Carlo mean-field will include the contribution from beams. Note that this approach will remove the subdominant contribution due to the $\Delta^{(2)}$ terms, as well as the $\Delta^{(1)}$ terms which we used for the analytical calculation, although we have verified numerically that the $\Delta^{(2)}$ terms do not contribute more than a few percent to the beam mean-field. For the convolution we use $s_{\max} = 2$, as higher terms do not contribute to the quadrupolar anisotropy. To obtain a minimum-variance estimator, we should also incorporate beam effects into the inverse-variance filtering operation, as discussed in the previous section, however we find that the estimator noise variance for the asymmetrically convolved simulations is less than 10% higher than that without beam effects, and so this improvement would not have a significant effect on our results.

The significance of the measured g_{2M} is plotted in Fig. 1 for the foreground-reduced WMAP V- and W-band DAs, incorporating all of the usable signal in the WMAP data by taking $l_{\max} = 1000$. It can be seen that the mean-field subtraction of beam effects results in data which are consistent with the isotropic model. The non-δ_{M0} values are very similar for all detectors, as one would expect for an isotropic sky, given that a large fraction of the estimator ''noise'' is due to the CMB fluctuations themselves, which are common between detectors. The variation for the δ_{M0} modes is more significant, indicating that there may be some small errors in the mean-field subtraction. The measured value of g_{20} is not significant in any detector, however, with the exception of $W4$ which shows a large negative bias even after subtraction of the beam mean-field. It should be kept in mind that without beam subtraction, each DA shows 6–9σ effects in the δ_{M0} modes. We believe that the residual anomaly in $W4$ may be attributed to the effects of correlated noise. The $W4$ DA has clearly correlated noise even after the prewhitening stage of the WMAP analysis [25]. Its $1/f$ knee frequency is several

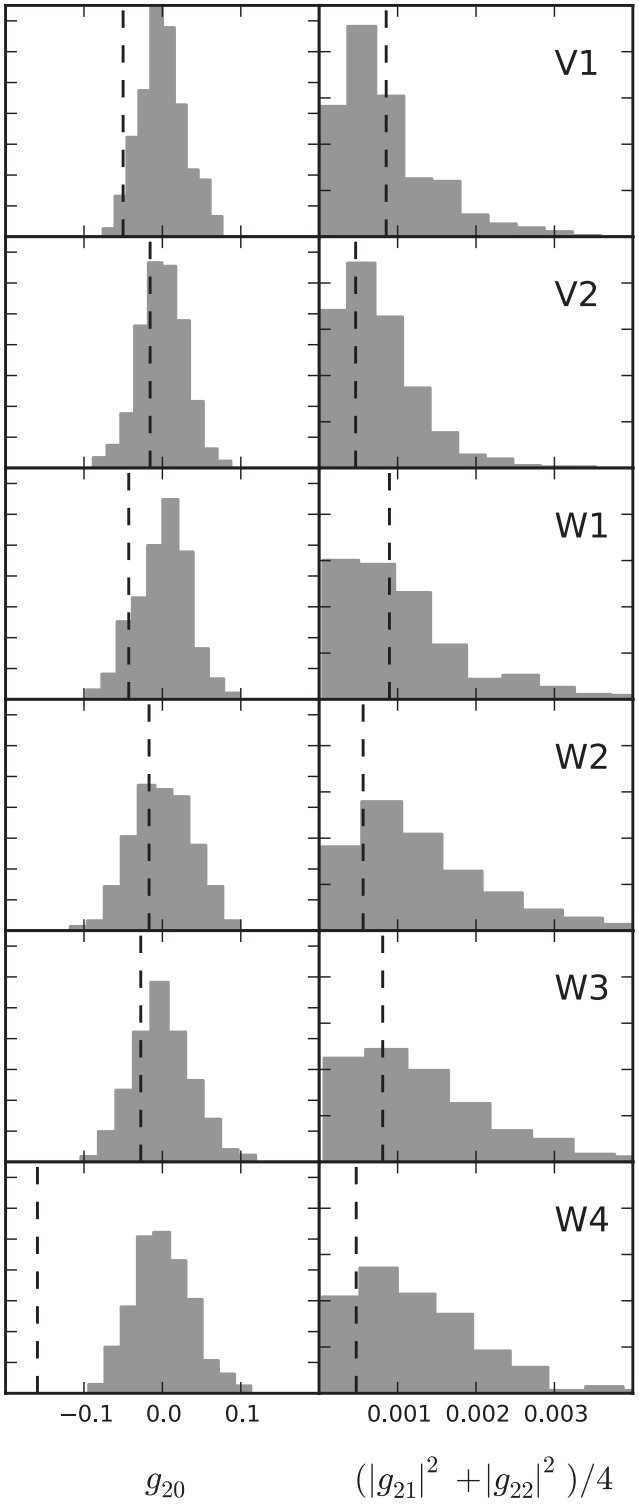

FIG. 1. Significance of the observed WMAP primordial-power-modulation quadrupole, with correction for beams, for the WMAP V-band foreground-reduced data, limited to $l_{\max} = 1000$. This is essentially a beam-corrected version of Fig. 9 in [15]. The gray histograms are from the 500 simulations which are used to determine the estimator Fisher matrix and mean-field. The dashed vertical lines are for the observed data. Detailed interpretation is provided in the text.

times larger than any of the other DAs [27]. A negative bias to g_{20} from correlated noise is also expected analytically. For subdominant correlated noise, the effects of striping can be modeled as a convolution of the pixel-uncorrelated instrumental noise with a narrow beam which has its semimajor axis along the scan direction. As we have already seen with the Q-band data, this leads to a negative bias in g_{20}. We can further test this hypothesis by forming our quadratic estimator from pairs of maps with uncorrelated noise. For this we use the $W4$ data for individual years. Autocorrelating the data for any single year and correcting for beam effects, we continue to find a large negative bias in g_{20} (albeit with slightly less statistical significance due to the larger instrumental noise for only a single year of data). Cross-correlating data from any pair of separate years, however, the effect disappears. Although we do not plot them here, the Q-band data are also completely consistent with $g_{20} = 0$ after correction for beam effects. We therefore assert that beam effects provide a sufficient explanation for the detected anomaly. Based on the average diagonal elements of our simulation Fisher matrices, we place a conservative limit on any single mode of $|g_{2M}| < 0.07$ at 95% confidence. The corresponding limit for the power spectrum of g_{2M} is $C_2^{gg} < 0.003$.

Disagreement with other results.—In [15] we tested the effect of beam asymmetries using the simulations of [1], which appeared only partially to explain the strong detected signal. However, on closer inspection, we find problems with these simulations, indicating that they are not representative of the effect of the WMAP beams. Applying the modulation estimator to these simulations with no noise, we find that they show a strong mean-field, with a spatial pattern which is identical between detectors, as expected analytically. The mean-field does not, however, have the purely planar structure associated with a δ_{M0} pattern in ecliptic coordinates. Such an error is most likely due to errors in the beam orientation angles α_i; however, private communication with Eriksen *et al.* has been unsuccessful in revealing the precise origin of this discrepancy. Our results are also discrepant with [19], who analyzed one of the simulations from [1] and found no beam effects. We believe this is due to two factors: (i) the simulation which they analyzed is one in which we also saw small effects in our original work [15]; and (ii) the nonplanar structure of the mean-field in the simulations poses difficulty for the estimator used by [19], which searches explicitly for the planar mode.

V. CONCLUSIONS

Beam asymmetry effects can be more important for anisotropy estimators than for power spectrum analysis, because their effects generally enter at lower order in the asymmetry. Beam asymmetries fit nicely into the larger formalism of quadratic anisotropy estimators. They result in a mean-field bias which directly traces the scan strategy ${}_sw_{LM}$, and can be calculated analytically on the full sky or determined from Monte-Carlo simulations on the cut sky.

Beam effects appear to provide a sufficient explanation for the 9σ detection of an apparent quadrupolar modulation of the primordial power spectrum in the WMAP data. We note that the WMAP team already incorporates the effects of beam asymmetry into their power spectrum analysis (where it is a much smaller effect in any case), and so the resolution of this anomaly should not have any effect on their cosmological parameter constraints.

All of this work will apply directly to the Planck experiment, which has a less symmetrizing scan strategy than WMAP. Planck's increased sensitivity also opens up the field for the precision analysis of interesting astrophysical secondaries such as the anisotropic signal from gravitational lensing. The tools and techniques which we have discussed here may also be extended straightforwardly for use with polarization data.

ACKNOWLEDGMENTS

Some of the results in this paper have been derived using HEALPIX [29]. We acknowledge the use of the Legacy Archive for Microwave Background Data Analysis (LAMBDA). Support for LAMBDA is provided by the NASA Office of Space Science. We thank Kendrick Smith, David Spergel, and Jo Dunkley for helpful comments on a draft version of this manuscript, as well as Hans Kristian Eriksen and Nicolaas Groeneboom for correspondence.

APPENDIX A: TOY SCAN STRATEGY

Here we consider a simple model of a scan strategy which serves as a good approximation to typical satellite experiments. It consists of:

(1) a beam at an angle θ_b to the satellite spin axis, which rotates with period τ_s;
(2) a precession at an angle θ_p to the antisolar direction, with period τ_p; and
(3) a continuous repointing of the antisolar direction as the observer orbits the sun.

If $\tau_s \ll \tau_p \ll 1$ year, then $w(\Omega_p, s)$ can be calculated analytically [7]. First, we calculate the quantity $v(\Omega_p, s) = \sum_{i \in p} e^{is\alpha_i}$ and then we form $w(\Omega_p, s) = v(\Omega_p, s)/v(\Omega_p, 0)$.

To calculate $v(\Omega_p, s)$, begin in a coordinate system which places the spacecraft spin axis along the $+z$ axis. Rotation about the spin axis in these coordinates gives $v^{(1)}(\Omega_p, s) \propto \delta(\theta - \theta_b)e^{is0}$. Expanding this using the appropriate spin harmonics gives

$$[v^{(1)}(\Omega_p, s)]_{lm} = K\delta_{m0s}Y_{l0}(\theta_b, 0), \tag{A1}$$

where K is some constant. We can then rotate out to place

the precession axis along the $+z$ axis, obtaining $v(p, s)$ in precession coordinates:

$$[v^{(2)}(\Omega_p, s)]_{lm} = \sum_{m''} D^l_{mm''}(0, \theta_p, 0)[v^{(1)}(\Omega_p, s)]_{lm''}. \quad \text{(A2)}$$

Rotation about the precession axis removes all but the $m = 0$ components giving

$$\begin{aligned}[v^{(2)}(\Omega_p, s)]_{lm} &= \delta_{m0} D^l_{00}(0, \theta_p, 0)[v^{(1)}(\Omega_p, s)]_{l0} \\ &= \delta_{m0} K P_l(\cos\theta_p)\, {}_sY_{l0}(\theta_b, 0). \end{aligned} \quad \text{(A3)}$$

Finally, the precession axis is rotated 90° down to the ecliptic plane, and again only $m = 0$ modes in the new coordinates are taken, to effect the azimuthal averaging given by the yearly rotation about the sun:

$$[v(\Omega_p, s)]_{lm} = \delta_{m0} K P_l(0) P_l(\cos\theta_p)\, {}_sY_{l0}(\theta_b, 0). \quad \text{(A4)}$$

This can be used to calculate $w(\Omega_p, s)$ in ecliptic coordinates. Note that only multipoles with l even are nonzero due to the north-south symmetry of the scan pattern. This is enforced by the dependence on $P_l(0)$.

APPENDIX B: BEAM ASYMMETRIES AND POWER SPECTRA

For the CMB temperature power spectrum, beam asymmetries are only important at high l (i.e. below the beam scale). On such scales, a pseudo-C_l analysis is usually employed in which a weight function is applied to the observed sky and the empirical (pseudo) power spectrum of the weighted sky is taken. The expectation value of the pseudo-C_l, after removal of the bias due to instrument noise, is linearly related to the true power spectrum, $C_l^{\Theta\Theta}$. In this Appendix, we calculate this relation in the presence of beam asymmetries; for related work see [11]. Good performance can be obtained from pseudo-C_l estimators with a careful choice of weight function [28], such as a local approximation to the optimal inverse signal-plus-noise weighting. Below the beam scale, the signal is exponentially suppressed and weighting by the inverse variance of the pixel noise is close to optimal.

We noted in Sec. II that, for full-sky observations and uniform weighting of the data, beam asymmetries only affect the power spectrum at second order. This is no longer true with anisotropic weighting, which generally will arise from the survey geometry or inhomogeneities in the noise. In this case, we generalize Eq. (7) to include a spin-0 pixel weight function on the right-hand side. Equation (8) then still holds, but ${}_0w_{LM}$ is no longer necessarily zero for $L \neq 0$. Writing the integral of three spin harmonics in terms of $3j$ symbols, we have

$$\begin{aligned}\tilde{\Theta}_{l'm'} = \sum_{LMS}\sum_{lm}(-1)^{m'}\sqrt{\frac{(2l+1)(2l'+1)(2L+1)}{4\pi}} \\ \times \begin{pmatrix} l' & l & L \\ -m' & m & M \end{pmatrix}\begin{pmatrix} l' & l & L \\ 0 & -S & S \end{pmatrix} B_{lS-S}\, {}_sw_{LM}\Theta_{lm}.\end{aligned} \quad \text{(B1)}$$

Inserting this in the definition of the pseudo power spectrum,

$$\tilde{C}_l \equiv \frac{1}{2l+1}\sum_m |\tilde{\Theta}_{lm}|^2, \quad \text{(B2)}$$

and taking the expectation value, we find

$$\begin{aligned}\langle\tilde{C}_l\rangle = \sum_{l'S'LS}\frac{(2l+1)(2L+1)}{4\pi}\begin{pmatrix} l' & l & L \\ 0 & -S & S \end{pmatrix} \\ \times \begin{pmatrix} l' & l & L \\ 0 & -S' & S' \end{pmatrix} B_{lS}B^*_{lS'(-S-S')}\,\mathcal{W}_L C_l^{\Theta\Theta},\end{aligned} \quad \text{(B3)}$$

where we have used an orthogonality relation for the $3j$ symbols. Here, the scan strategy and weight function are encoded in the cross spectra

$${}_{(SS')}\mathcal{W}_L \equiv \frac{1}{2L+1}\sum_M {}_sw_{LMS'}\, {}_sw^*_{LM}. \quad \text{(B4)}$$

For mildly asymmetric beams, or a wide distribution of crossing angles, the sums over S and S' in Eq. (B3) can be truncated after only a few terms. In this case, the effect of beam asymmetries on the mean pseudo-C_l can be computed efficiently with no further simplifying assumptions.

For the case of symmetric beams ($B_{lS} = \delta_{S0}B_{l0}$), or for a uniform distribution of observation angles in each pixel (${}_sw_{LM} = {}_sw_{LM}\delta_{S0}$), Eq. (B3) reduces to the usual result [28] for symmetric beams.

[1] I. K. Wehus, L. Ackerman, H. K. Eriksen, and N. E. Groeneboom, Astrophys. J. **707**, 343 (2009).
[2] T. Souradeep and B. Ratra, Astrophys. J. **560**, 28 (2001).
[3] D. A. Varshalovich, A. N. Moksalev, and V. K. Khersonskii, *Quantum Theory of Angular Momentum* (World Scientific Publishing Co., Singapore, 1988).
[4] B. D. Wandelt and K. M. Gorski, Phys. Rev. D **63**, 123002 (2001).
[5] M. Tristram, J.-C. Hamilton, J. F. Macias-Perez, and C. Renault, Phys. Rev. D **69**, 123008 (2004).
[6] K. M. Smith, O. Zahn, and O. Dore, Phys. Rev. D **76**, 043510 (2007).

[7] C. M. Hirata, N. Padmanabhan, U. Seljak, D. Schlegel, and J. Brinkmann, Phys. Rev. D **70**, 103501 (2004).
[8] C. M. Hirata, S. Ho, N. Padmanabhan, U. Seljak, and N. A. Bahcall, Phys. Rev. D **78**, 043520 (2008).
[9] S. Mitra, A. S. Sengupta, and T. Souradeep, Phys. Rev. D **70**, 103002 (2004).
[10] C. Armitage and B. D. Wandelt, Phys. Rev. D **70**, 123007 (2004).
[11] G. Hinshaw *et al.* (WMAP Collaboration), Astrophys. J. Suppl. Ser. **170**, 288 (2007).
[12] A. Lewis and A. Challinor, Phys. Rep. **429**, 1 (2006).
[13] C. Dvorkin and K. M. Smith, Phys. Rev. D **79**, 043003 (2009).
[14] A. Challinor and F. van Leeuwen, Phys. Rev. D **65**, 103001 (2002).
[15] D. Hanson and A. Lewis, Phys. Rev. D **80**, 063004 (2009).
[16] A. Hajian and T. Souradeep, Astrophys. J. **597**, L5 (2003).
[17] C. L. Bennett *et al.*, arXiv:1001.4758.
[18] D. Hanson, G. Rocha, and K. Gorski, Mon. Not. R. Astron. Soc. **400**, 2169 (2009).
[19] N. E. Groeneboom, L. Ackerman, I. K. Wehus, and H. K. Eriksen, arXiv:0911.0150.
[20] L. Ackerman, S. M. Carroll, and M. B. Wise, Phys. Rev. D **75**, 083502 (2007).
[21] C. G. Boehmer and D. F. Mota, Phys. Lett. B **663**, 168 (2008).
[22] N. E. Groeneboom and H. K. Eriksen, Astrophys. J. **690**, 1807 (2009).
[23] A. R. Pullen and M. Kamionkowski, Phys. Rev. D **76**, 103529 (2007).
[24] G. Hinshaw *et al.* (WMAP Collaboration), Astrophys. J. Suppl. Ser. **180**, 225 (2009).
[25] G. Hinshaw *et al.* (WMAP Collaboration), Astrophys. J. Suppl. Ser. **148**, 63 (2003).
[26] L. Page *et al.* (WMAP Collaboration), Astrophys. J. Suppl. Ser. **148**, 39 (2003).
[27] N. Jarosik *et al.* (WMAP Collaboration), Astrophys. J. Suppl. Ser. **148**, 29 (2003).
[28] G. Efstathiou, Mon. Not. R. Astron. Soc. **349**, 603 (2004).
[29] K. M. Gorski *et al.*, Astrophys. J. **622**, 759 (2005).